

On the association between spring Arctic sea ice concentration and Chinese summer rainfall

Bingyi Wu,¹ Renhe Zhang,¹ Bin Wang,² and Rosanne D'Arrigo³

Received 14 January 2009; revised 26 February 2009; accepted 12 March 2009; published 5 May 2009.

[1] A statistical relationship between spring Arctic sea ice concentration (SIC) and Chinese summer rainfall is identified using singular value decomposition (SVD). Results show that decreased (increased) spring SIC in the Arctic Ocean and the Greenland Sea corresponds to increased (decreased) summer rainfall in northeast China and central China between the Yangtze River and the Yellow River (28°–36°N); and decreased (increased) rainfall in south China. Corresponding summer 500 hPa height anomalies show a Eurasian wave train structure, which originates in northern Europe and extends southeastwards to northeast China, and a south-north dipole structure over East Asia south to Lake Baikal. Such a spatial distribution of 500 hPa height anomalies and corresponding summer rainfall anomalies cannot be entirely attributed to the impact of East Asian summer monsoon (EASM) variability. The spring Arctic SIC provides a complementary precursor for Chinese summer rainfall variability. The combined impacts of both spring Arctic SIC and Eurasian snow cover on the Eurasian wave train may explain their statistical linkage. **Citation:** Wu, B., R. Zhang, B. Wang, and R. D'Arrigo (2009), On the association between spring Arctic sea ice concentration and Chinese summer rainfall, *Geophys. Res. Lett.*, 36, L09501, doi:10.1029/2009GL037299.

1. Introduction

[2] The role of Arctic sea ice in the Earth's climate system has been extensively investigated using observations and simulations [Walsh, 1983; Honda *et al.*, 1996; Rigor *et al.*, 2002; Alexander *et al.*, 2004; Deser *et al.*, 2004; Magnusdottir *et al.*, 2004; Wu *et al.*, 2004]. Yet, the association of Arctic sea ice with Chinese summer rainfall and East Asian summer monsoon (EASM) is still unclear and not well studied. Limited research [Niu *et al.*, 2003] has shown that reduced spring sea ice extent in the Bering and Okhotsk seas corresponds to enhanced June–July rainfall in southeast China. However, spring sea ice variability is generally out of phase between the Bering and Okhotsk seas, thus grouping them together is inappropriate [Cavalieri and Parkinson, 1987; Fang and Wallace, 1994]. The motivation of this study is to assess potential predictors for Chinese summer rainfall variations. We therefore investigate a statistical linkage between Arctic sea ice variability in the

boreal spring (March–May) and Chinese summer rainfall. Because Arctic sea ice concentration (SIC) variations typically have a more substantial impact on the atmospheric circulation than sea ice extent variations [Alexander *et al.*, 2004] we focus herein on spring Arctic SIC variability.

2. Data and Method

[3] The primary datasets used in this study are the monthly mean Arctic SIC dataset (on a 1° latitude × 1° longitude grid for the period 1961–2007), obtained from the British Atmospheric Data Centre (BADC, <http://badc.nerc.ac.uk/data/hadisst/>), and a monthly 513-station rainfall dataset for China, obtained from the National Meteorological Information Centre of China, spanning the period from 1968 to 2005. The sea level pressure (SLP), 850 hPa winds, and 500 hPa geopotential heights are obtained from the National Center for Environmental Prediction (NCEP) and the National Center for Atmospheric Research (NCAR) reanalysis datasets for the period of 1968–2007. The monthly mean snow water equivalent (SWE) dataset was derived from National Snow and Ice Center during the period from 1979 to 2004 [Armstrong *et al.*, 2005]. The SWE data have been converted to 1° × 1° grids in this study.

[4] To reveal the dominant modes of co-variability between spring Arctic SIC and Chinese summer rainfall, we used the singular value decomposition (SVD) method. Additionally, we applied empirical orthogonal function (EOF) analysis (based on the correlation matrix) to extract, respectively, dominant modes of spring Arctic SIC variability and Chinese summer rainfall variability. In this study, we focus on interannual variability of the seasonal means, averaged for three spring (March–May) and three summer (June–August) months.

3. A Statistical Linkage Between Spring Arctic SIC and Chinese Summer Rainfall

[5] Figure 1 shows the time series and corresponding spatial distributions of the leading SVD between spring Arctic SIC and China summer rainfall, which accounts for 19% of their co-variance. Both Arctic SIC and summer rainfall in the leading SVD display a coherent interannual variability (the correlation is 0.83, Figure 1a) and apparent interdecadal variations with turning points occurring around 1978 and 1992, respectively. For spring SIC, negative phases were frequent during the periods 1968–1978 and 1993–2005, and separated by dominant positive phases. The corresponding SIC anomalies were positive in most of Eurasian marginal seas, with negative SIC anomalies in the Arctic Basin, the Beaufort Sea, and the Greenland Sea

¹Chinese Academy of Meteorological Sciences, China Meteorological Administration, Beijing, China.

²Department of Meteorology and International Pacific Research Center, University of Hawaii at Manoa, Honolulu, Hawaii, USA.

³Tree-Ring Laboratory, Lamont-Doherty Earth Observatory, Palisades, New York, USA.

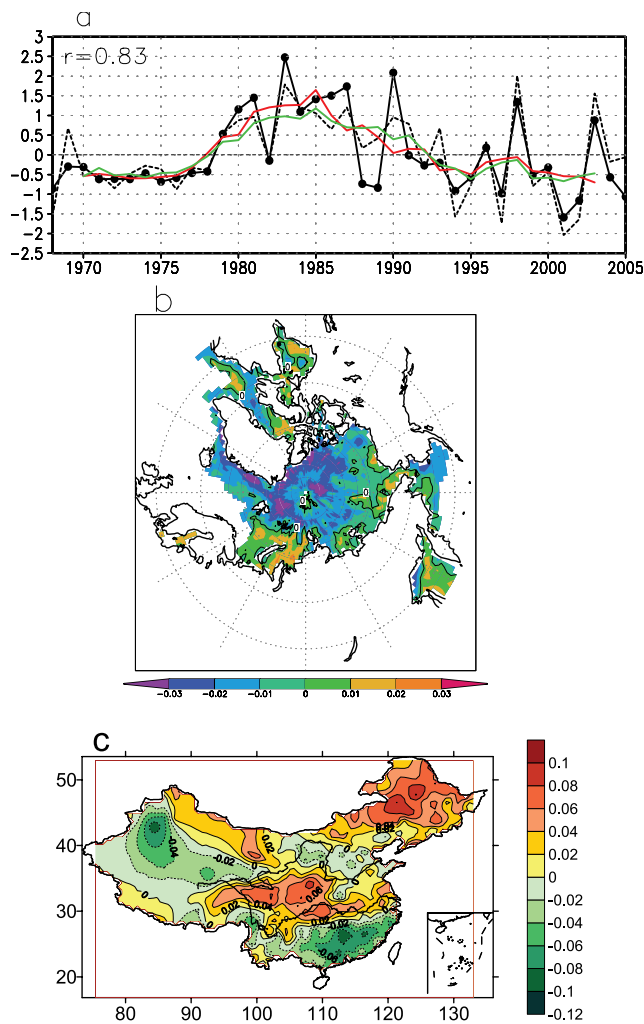


Figure 1. (a) Normalized time series of spring Arctic SIC (solid line) and summer rainfall (dashed line) variations in the leading SVD, the red and green lines denote their 5-year running means, respectively, (b) the spatial distribution of spring Arctic SIC variations in the leading SVD, (c) same as Figure 1b but for the summer rainfall variations. In Figures 1b and 1c units are arbitrary.

during 1979–1992. Opposite SIC anomalies occurred during the periods 1968–1978 and 1993–2005 (Figure 1b). It is worth noting that spring SIC variability is out of phase in the Bering Sea and the Okhotsk Sea. During the period 1979–1992, positive rainfall anomalies frequently appeared in northeast China and central China between the Yangtze River and the Yellow River (28° – 36° N), with negative rainfall anomalies in south and southeast China (Figure 1c). Opposing spatial distribution of summer rainfall anomalies frequently occurred in the period 1968–1978 and 1993–2005. Ding *et al.* [2007] examined interdecadal variations of Chinese summer rainfall over the past five decades and found that 1978 and 1992 are two abrupt climate change points, which is well consistent with our results.

[6] The heterogeneous correlations for the leading SVD show significant negative correlations in the Arctic Ocean, the Greenland Sea (Figure 2a). For summer rainfall, significant positive correlations are seen in northeast China and

central China between the Yangtze and the Yellow Rivers, with significant negative correlations in south and southeast China (Figure 2b). These results imply that decreased spring SIC in the Arctic Ocean and the Greenland Sea tends to be

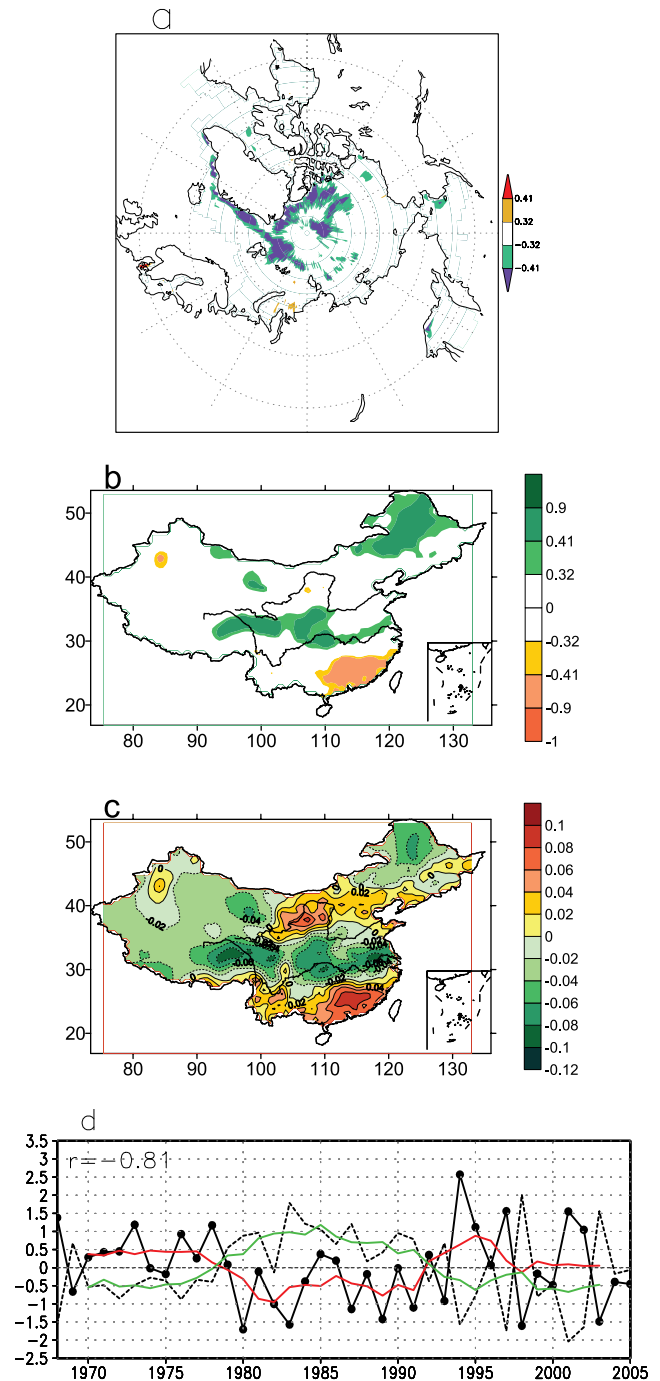


Figure 2. (a) The spatial distribution of spring Arctic SIC heterogeneous correlations, the shading areas denote correlations at the 0.05 and 0.01 significance levels, respectively, (b) same as in Figure 2a but for Chinese summer rainfall, (c) the spatial distribution of the leading EOF of Chinese summer rainfall (Units: arbitrary), (d) normalized time series of both the leading EOF of summer rainfall (solid line) and summer rainfall variations in the leading SVD (dashed line), the red and green lines denote their 5-year running means, respectively.

associated with increased summer rainfall in northeast China and central China between the Yangtze and the Yellow Rivers and decreased summer rainfall in south and southeast China.

[7] We applied EOF analysis to spring SIC during the period 1961–2007. The first two EOFs account for 13% and 10% of the variance, respectively. According to *North et al.* [1982], the first three EOFs are well separated from each other. In fact, the leading EOF reflects the overall decline trend in sea ice associated with global warming (not shown). The second EOF of spring Arctic SIC variability closely resembles Figure 1b but with opposite sign (not shown). The correlation between the second EOF and spring SIC variations in the leading SVD is -0.95 . Thus spring SIC variations in the leading SVD reflect a dominant pattern of spring SIC variability.

[8] Similarly, we extracted the leading EOF of Chinese summer rainfall variability, which accounts for 10% of the variance during the period 1968–2005. The spatial distribution and temporal evolution of the leading rainfall EOF closely resemble Figures 1c and 1a, respectively, but with opposite sign (Figures 2c and 2d). The correlation between them is -0.81 . On interdecadal time-scales, negative phases are dominant during the period 1979–1991, in contrast to opposite phases before and after (Figure 2d). Consequently, summer rainfall variation in the leading SVD is significantly correlated with the leading rainfall EOF.

[9] In fact, the spatial distribution of the leading rainfall EOF can be attributed to the combination effect of two wave trains in summer 500 hPa height anomalies (Figure 3a). The first wave train shows a meridional structure along the East Asian coast, with two negative anomalous centers over southeast China and the Okhotsk Sea and a positive anomalous center between them when the rainfall pattern is in its positive phase. The wave train closely resembles the Pacific-Japan pattern [Nitta, 1987; Huang and Li, 1987], which is closely related to EASM variability [Wang et al., 2001; Wu et al., 2008]. The second wave train originates from northern Europe extending southeastwards to Korean Peninsula. There are three anomalous centers over northern Europe, northwestern Asian continent and northeast Asia. Correspondingly, summer 850 hPa wind anomalies show an anomalous cyclone over south and southeast China and an anomalous anticyclone over northeast Asia (Figure 3b). Figure 3b shows opposing expressions of EASM variability in north China and south and southwest China. There is an anomalous anticyclone over northeast China, leading to decreased summer rainfall there (Figure 3c). Divergences in anomalous 850 hPa winds seem to appear over the Yangtze River valley, with an anomalous cyclone over 37.5° – 50° N, 90° – 110° E. Such a spatial distribution of summer 850 hPa wind anomalies is dynamically consistent with significantly increased rainfall in the mid-reaches of the Yellow River valley, southwest, south and southeast China; with significantly decreased rainfall in northeast China, the mid-low reaches of Yangtze River (Figure 3c).

[10] Figure 3d shows the 500 hPa height anomalies associated with the circulation index of the western North Pacific (WNP) and EASM proposed by Wang and Fan [1999]. The Wang-Fan index describes the precipitation variability in the WNP monsoon trough, which drives subtropical and extratropical EASM variability through

the meridional tri-pole teleconnection (Figure 3d). The Wang-Fan index captures the tri-pole wave train very well, however, it cannot completely capture the Eurasian wave train shown in Figure 3a, and two anomalous centers over south of 50° N migrate eastwards relative to that in Figure 3a. Corresponding 850 hPa wind anomalies obviously differ from that in Figure 3b, particularly over area from north China to Lake Baikal where wind anomalies are very weak, leading to significantly decreased rainfall along the Yangtze River valley, the low-reaches of the Yellow River and northeast China and moderate increased rainfall in parts of south and southeast China (Figure 3f). Although the leading rainfall EOF is significantly correlated with the Wang-Fan index ($r = 0.43$, at the 0.01 significance level) and corresponding height anomalies show the great similarity along the East Asian coast region WNP-EASM cannot completely explain the spatial distribution of summer rainfall anomalies associated with the leading rainfall EOF, particularly in north China.

[11] Summer 500 hPa height anomalies associated with the preceding spring Arctic SIC also show the Eurasian wave train originating from northern Europe and extending southeastwards to southeast of Lake Baikal region and northeast China (Figure 3g). Height anomalies exhibit a south-north dipole structure south of Lake Baikal. An anomalous cyclone over northeast China and an anomalous anticyclone over south China are concurrent, with strong convergences over the Yangtze River valley (Figure 3h). Thus, significantly increased rainfall can be observed in northeast China and central China between the Yangtze River and the Yellow River, and significantly decreased rainfall in south and southeast China (Figure 3i). Since the Wang-Fan index reflects WNP-EASM variability that is dominated by ENSO, the results here suggested that the spring Arctic SIC provides a precursor for Chinese summer rainfall variability that is complementary to the effects of ENSO. Although spring Arctic SIC and Chinese summer rainfall exhibit coherent interannual and interdecadal variations their association on interannual time scales is more important relative to interdecadal time scales (not shown).

4. Possible Linkage Mechanisms and Discussion

[12] We only attempt to explain the possible reason for the Eurasian wave train. In fact, variations in spring Arctic SIC and Eurasian snow cover are coherent, which is reflected in significant positive correlations between spring Arctic SIC in the leading SVD and the gridded SWE in northern Eurasia (not shown). This result implies that decreased Arctic SIC in the Arctic Ocean and the Greenland Sea and increased SIC in most of Eurasian marginal seas (Figure 1b) correspond to excessive spring Eurasian SWE. The spring regionally-averaged SWE (55° – 75° N and 60° – 120° E) is broadly similar to Arctic SIC variations in the leading SVD ($r = 0.64$, at the 0.01 significance level), but individual springs can be radically different (Figure 4a). The evolution of 500 hPa height anomalies from spring to summer associated with spring Eurasian SWE is illustrated in Figures 4b and 4c, which show composite differences between above ($\sigma > 0.8$: 1979, 1980, 1983, 1984, 1985, 1987, 1996) and below-normal Eurasian SWE ($\sigma < -0.8$: 1990, 1995, 1997, 2001, 2002). Positive anomalies in spring

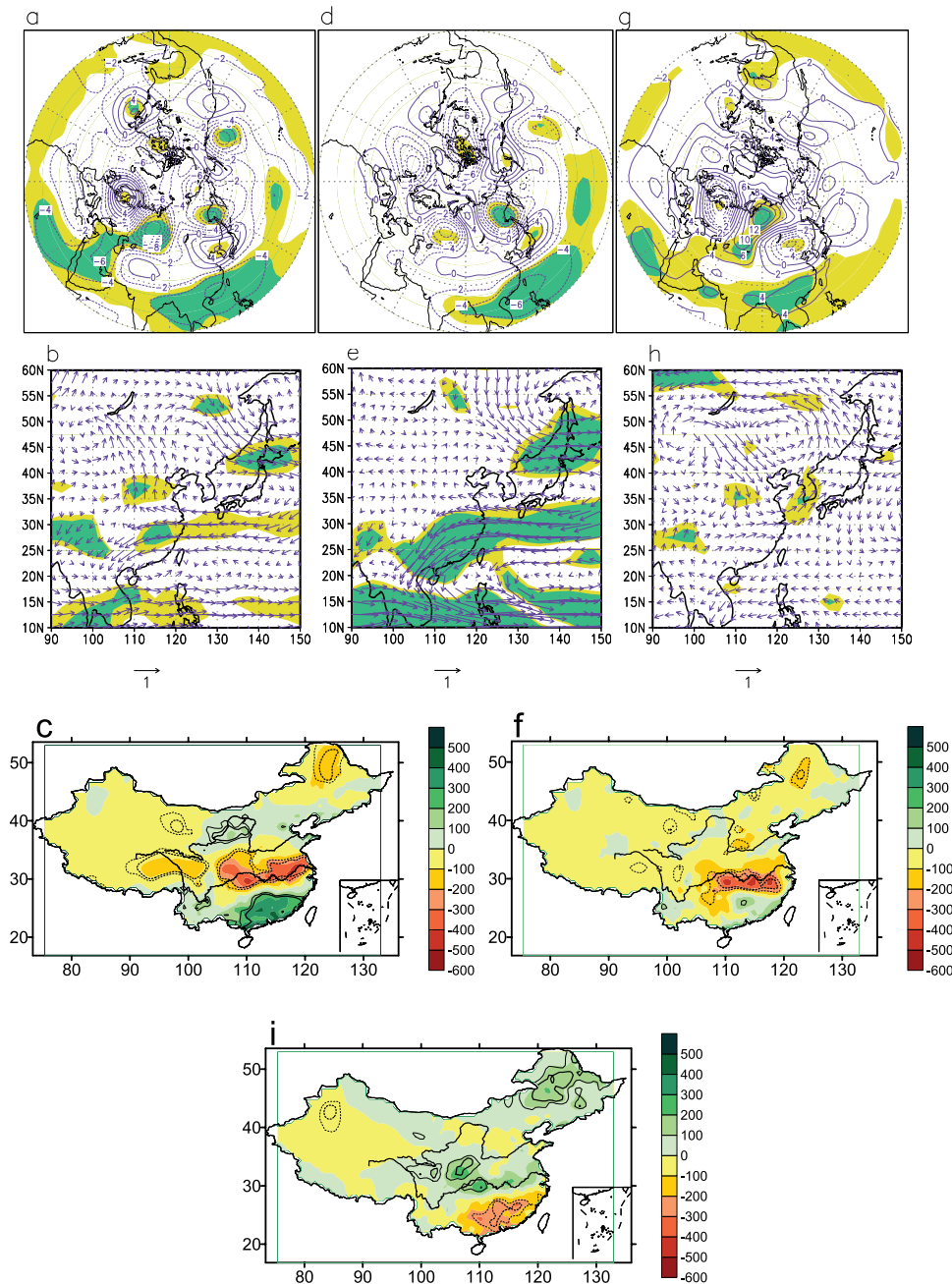


Figure 3. Summer anomalies in (a) 500 hPa height, (b) 850 hPa wind, and (c) Chinese summer rainfall, derived from regressions on the leading EOF of Chinese summer rainfall variability, in Figures 3a and 3b, the shading areas represent height and wind velocity anomalies exceed the 0.05 and 0.01 confidence levels, respectively, in Figure 3c, thin and thick lines denote that rainfall anomalies are above the 0.05 and 0.01 confidence levels, respectively. Units: in Figure 3c, gpm; in Figure 3b, m/s; in Figure 3c, 0.1 mm. (d–f and g–i) same as Figures 3a–3c, respectively, but derived from the circulation index of Wang and Fan [1999] and spring Arctic SIC signs in the leading SVD.

Eurasian SWE correspond to three anomalous centers, respectively, over the western and northern Europe, and northwest of Lake Baikal (Figure 4b). The three anomalous centers then migrate, respectively, to the northern Europe, northwest Asia continent close to the Kara Sea, and southeast of Lake Baikal (Figure 4c). Figure 4c closely resembles Figure 3g but with strengthened amplitudes, reflecting the combined effect of both spring Arctic SIC and Eurasian SWE [Yasunari *et al.*, 1991]. The simulation result partly

supports this hypothesis [Dethloff *et al.*, 2006]. It should be pointed out that differences in analysis approach and data length are likely to induce the difference in amplitude in Figures 3g and 4c.

[13] It is very difficult, however, to directly detect the impact of sea ice on the atmosphere because of dominant roles of atmospheric forcing on sea ice [Deser *et al.*, 2000; Wu *et al.*, 2004]. We speculate that surface wind forcing determines spring SIC anomalies, which largely persist until

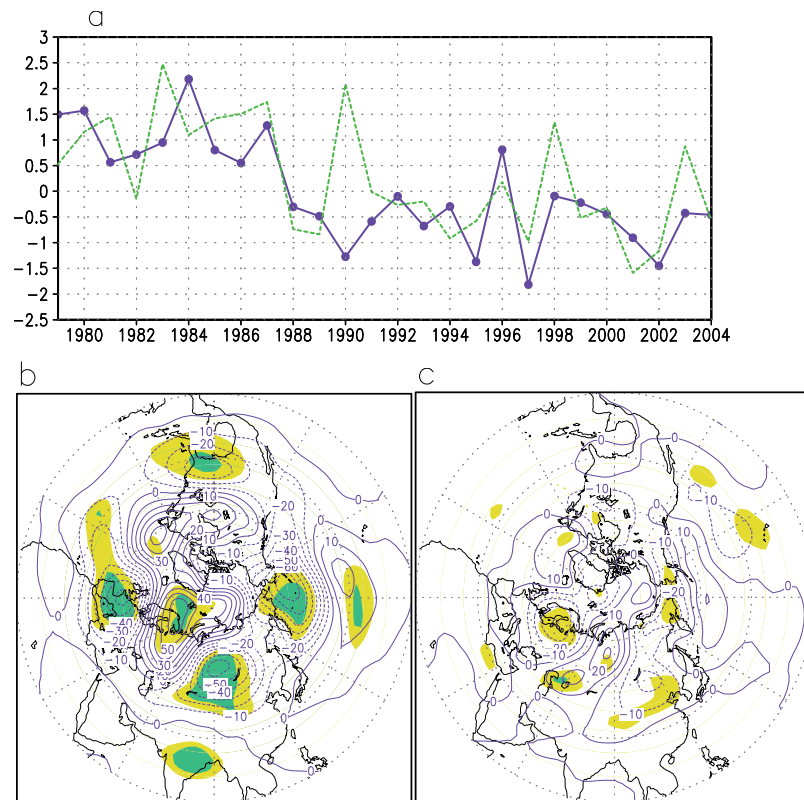


Figure 4. (a) Normalized time series of spring regionally averaged snow water equivalent (55° – 75° N and 60° – 120° E) (purple line) and spring Arctic SIC in the leading SVD, (b) composite differences in spring mean 500 hPa heights between excessive and less snow water equivalent (for composite cases, see the text), the shading areas denote that differences exceed the 0.05 and 0.01 confidence levels, respectively, (c) same as Figure 4b but for summer. In Figures 4b and 4c, units are gpm.

the following summer. In turn, the accumulated impact of persistent SIC anomalies from spring to summer could impact the summer subpolar westerlies through changing albedo and heat flux between the atmosphere and ocean, which further influences redistribution of Rossby waves (Figure 3g). The precise mechanism responsible for their associations needs to be further investigated through observations and simulations in the future.

[14] **Acknowledgments.** This study was supported by the National Key Basic Research and Development Project of China (grants 2004CB418300 and 2007CB411505), Chinese COPES project (GYHY200706005) and the National Natural Science Foundation of China (grant 40875052).

References

- Alexander, M. A., et al. (2004), The atmospheric response to realistic sea ice anomalies in an AGCM during winter, *J. Clim.*, **17**, 890–905.
- Armstrong, R. L., M. J. Brodzik, K. Knowles, and M. Savoie (2005), Global Monthly EASE-Grid Snow Water Equivalent Climatology, <http://nsidc.org/data/nsidc-0271.html>, Natl. Snow and Ice Data Cent., Boulder, Colo.
- Cavalieri, D. J., and C. L. Parkinson (1987), On the relationship between atmospheric circulation and fluctuations in sea ice extents of the Bering and Okhotsk Seas, *J. Geophys. Res.*, **92**, 7141–7162.
- Dethloff, K., et al. (2006), A dynamical link between the Arctic and the global climate system, *Geophys. Res. Lett.*, **33**, L03703, doi:10.1029/2005GL025245.
- Deser, C., J. E. Walsh, and M. S. Timlin (2000), Arctic sea ice variability in the context of recent atmospheric circulation trends, *J. Clim.*, **13**, 617–633.
- Deser, C., G. Magnusdottir, R. Saravanan, and A. Phillips (2004), The effects of North Atlantic SST and sea ice anomalies on the winter circulation in CCM3. Part II: Direct and indirect components of the response, *J. Clim.*, **17**, 877–889.
- Ding, Y., Z. Wang, and Y. Sun (2007), Inter-decadal variation of the summer precipitation in East China and its association with decreased Asian summer monsoon. Part I: Observational evidences, *Int. J. Climatol.*, **28**, 1139–1161, doi:10.1002/joc.1615.
- Fang, Z., and J. M. Wallace (1994), Arctic sea ice variability on a timescale of weeks: Its relation to atmospheric forcing, *J. Clim.*, **7**, 1897–1913.
- Honda, M., K. Yamazaki, Y. Tachibana, and K. Takeuchi (1996), Influence of Okhotsk sea-ice extent on atmospheric circulation, *Geophys. Res. Lett.*, **23**, 3595–3598.
- Huang, R., and W. Li (1987), Influence of the heat source anomaly over the western tropical Pacific on the subtropical high over east Asia, in *Proceedings of the International Conference on the General Circulation of East Asia*, pp. 40–51, Chengdu, China.
- Magnusdottir, G., C. Deser, and R. Saravanan (2004), The effects of North Atlantic SST and sea ice anomalies on the winter circulation in CCM3. Part I: Main features and storm track characteristics of the response, *J. Clim.*, **17**, 857–876.
- Nitta, T. (1987), Convective activities in the tropical western Pacific and their impacts on the Northern Hemisphere summer circulation, *J. Meteorol. Soc. Jpn.*, **65**, 165–171.
- Niu, T., P. Zhao, and L. Chen (2003), Effects of the sea-ice along the North Pacific on summer rainfall in China, *Acta Meteorol. Sin.*, **17**, 52–64.
- North, G. R., T. L. Bell, R. F. Cahalan, and F. J. Moeng (1982), Sampling errors in the estimation of EOFs, *Mon. Weather Rev.*, **110**, 699–706.
- Rigor, I. G., J. M. Wallace, and R. L. Colony (2002), Response of sea ice to the Arctic Oscillation, *J. Clim.*, **15**, 2648–2663.
- Walsh, J. E. (1983), Role of sea ice in climate variability: Theories and evidence, *Atmos. Ocean*, **21**, 229–242.
- Wang, B., and Z. Fan (1999), Choice of south Asian summer monsoon indices, *Bull. Am. Meteorol. Soc.*, **80**, 629–638.

- Wang, B., R. Wu, and K. Lau (2001), Interannual variability of the Asian summer monsoon: Contrasts between the Indian and the western North Pacific–east Asian monsoon, *J. Clim.*, *14*, 4073–4090.
- Wu, B., J. Wang, and J. Walsh (2004), Possible feedback of winter sea ice in the Greenland and the Barents Sea on the local atmosphere, *Mon. Weather Rev.*, *132*, 1876–1968.
- Wu, B., R. Zhang, Y. Ding, and R. D’Arrigo (2008), Distinct modes of the east Asian summer monsoon, *J. Clim.*, *21*, 1122–1138.
- Yasunari, T., A. Kitoh, and T. Tokioka (1991), Local and remote responses to excessive snow mass over Eurasia appearing in the northern spring and summer climate: A study with the MRI-GCM, *J. Meteorol. Soc. Jpn.*, *69*, 473–487.
-
- R. D’Arrigo, Tree-Ring Laboratory, Lamont-Doherty Earth Observatory, 61 Route 9W, Palisades, NY 10964, USA.
- B. Wang, Department of Meteorology and International Pacific Research Center, University of Hawaii at Manoa, 1680 East West Road, Post Building 401, Honolulu, HI 96822-2219, USA.
- B. Wu and R. Zhang, Chinese Academy of Meteorological Sciences, China Meteorological Administration, No. 46 Zhong-Guan-Cun South Avenue, Beijing 100081, China. (wby@cma.cma.gov.cn)